Resorbable defect analog PLGA scaffolds using CO_2 as solvent: Structural characterization

F. A. Maspero,[1,2] K. Ruffieux,[1,2] B. Müller,[1]* E. Wintermantel[1,3]
[1]*Biocompatible Materials Science and Engineering, ETH Zürich, Wagistrasse 23, CH-8952 Schlieren, Switzerland*
[2]*Degradable Solutions AG, Wagistrasse 23, CH-8952 Schlieren, Switzerland*
[3]*Zentralinstitut für Medizintechnik der TU München. Boltzmannstrasse 15, D-85748 Garching, Germany*

Received 1 June 2001; revised 25 September 2001; accepted 4 December 2001

Abstract: After tooth extraction, the immediate wound treatment by implanting an exact copy of the root could prevent alveolar bone atrophy. The implant should have an interconnected porosity in order to promote tissue in-growth. This communication reports a novel method to realize such net-shaped porous scaffolds fabricated within a few minutes. Porosity and micro-architecture are evaluated by Hg-porosimetry and by image analysis of electron and light microscopy as well as by computed micro-tomography. The total porosity of the scaffold corresponds to (63 ± 3)%, mainly related to open interconnected porosity. Micro-tomography, as a noninvasive 3D method, is best suited to uncover pores of about 100 μm, a diameter especially important for tissue in-growth. The differentiation between open and closed porosity, however, depends on the method chosen. This effect is attributed to the spherical pores with an orifice only detected in the 3D analysis. Consequently, the closed porosity is overestimated by 8% evaluating 2D images. Finally, the mean pore diameter is found to be 106 and 100 μm for 2D and 3D analysis, respectively. Although the porosity of the scaffold needs to be further optimized for clinical applications, the procedure proposed is a promising route in manufacturing open porous implants without the use of any organic solvent. © 2002 Wiley Periodicals, Inc. J Biomed Mater Res 62: 89–98, 2002

Key words: PLGA; interconnected porosity; image analysis; tooth root replica

INTRODUCTION

The extraction of teeth causes a major trauma for the alveolar ridge by leaving an open bone wound, which is in direct contact with the environment of the mouth. Subsequently, the bone atrophy often observed leads to a reduction of ridge height and width.[1,2] This atrophy may result in the loss of functionality of the bone as well as in potential bacterial contamination. In addition, the resorption of alveolar bone can lead to complications making reconstructive surgery necessary.[3] Although this problem had been described already in the last century,[4] therapies have only been evaluated seriously during the last two decades.[4] In previous studies,[4,5] prevention of resorption has been attempted by implanting dense hydroxyapatite cones into the alveola. Although these implants partially promoted the alveolar ridge stability, some post-implantation problems occurred, such as submucosal prominence, erosion through mucosa, and consequently the migration and the loss of the implant.[6] Moreover, the procedure necessitated fastidious mechanical adjustment of the implants that finally still fitted poorly into the extraction socket.

Recently, Suhonen and Meyer[7] have proposed immediate wound closure by placing an exact copy of the extracted tooth root made of a degradable polymer into the socket. The authors demonstrated the preservation of ridge height for at least 21 months. Although cancellous bone was observed at the implantation site, bone formation could only be initiated once the polymer implant had been at least partially resorbed. One potential approach to facilitate earlier tissue formation is the implantation of the biodegradable implant with interconnected pores that enable immediate tissue in-growth. As confirmed by several *in vitro* and *in vivo* studies,[8,9] open interconnected pores promote scaffold vascularization, which permits improved cell spreading and proliferation. According to the results of

*Present address: Computer Vision Laboratory, ETH Zürich, Gloriastrasse 35, CH-8092 Zürich, Switzerland
Correspondence to: B. Müller; e-mail: bmueller@vision.ee.ethz.ch

Contract grant sponsor: Swiss National Commission for Technology and Innovation; contract grant number: 4120.1

Ishaug et al.,[10] the optimal migration of osteoblasts and the preservation of their phenotype require scaffolds with pores having diameters larger than 100 μm.

Among the biodegradable polymers used in human surgery and tissue engineering, poly(α-hydroxy esters) such as polylactide, polyglycolide, and their copolymers (PLGA) are most frequently investigated.[11–18] They seem to be suitable materials for the preparation of porous defect-analog scaffolds. Several techniques are proposed in the literature to manufacture open porous scaffolds, including solvent casting/salt leaching,[19] phase separation,[20] gel casting,[21] precipitation,[22] and emulsion freeze-drying.[14] Many of these methods require organic solvent purification steps that are time consuming and consequently may make the fabrication of defect analogous scaffolds for immediate implantation impossible. Foaming techniques currently used to produce micro-cellular structures with gaseous CO_2 are fast, but do not give rise to sufficiently interconnected porosity required for cell in-growth. Harris et al.[23] have proposed an alternative method, combining salt leaching and CO_2 foaming. Here, however, salt removal needs to be considered.

On the basis of a procedure recently designed,[7,24] we propose an improved method to produce PLGA open scaffolds. This method, which involves rapid consolidation of PLGA particles in a mold using sub-critical CO_2, permits the fast preparation of an exact copy of a tooth root without the use of any organic solvent. After the detailed description of the PLGA scaffold preparation by consolidation of particles using sub-critical CO_2, the porous structure is characterized. The results obtained by standard techniques (gravimetry and Hg-porosimetry) are compared with those obtained by 2D and 3D image analysis using confocal laser scanning microscopy (CLSM) and synchrotron-radiation-based computed microtomography (CMT).

MATERIALS AND METHODS

Scaffold preparation

Poly(D,L-lactic-*co*-glycolic acid) (Boehringer-Ingelheim, D) particles were prepared as follows: PLGA fibers were spun at 15 m/s with a laboratory extruder (CSI Max Mixing Extruder CS 194 A) through a 3-mm diameter dye. These parameters lead to a thread diameter of about 70 μm. The PLGA threads were subsequently relaxed in a high-pressure CO_2 vessel (CO_2 medical grade, AGA, CH) at 55×10^5 Pa for 15 s. Then, the gas pressure was decreased from 55 to 1 10^5 Pa within about 20 s. During this treatment, the relaxing PLGA fibers formed aggregates. These aggregates were milled and sieved to a grain size of 700–1400 μm to obtain the base material for scaffold fabrication. Scaffolds were produced as follows: an aluminum cylindrical mold with a height of 20 mm and a diameter of 10 mm was filled with 0.15 g of PLGA particles placed into the CO_2 vessel. This amount of particles was consolidated using the same time-pressure ramps as described for the production of aggregates. Finally, open porous scaffolds with a diameter of 10 mm and a height of 5 mm were obtained. For these scaffolds, we have found an E-modulus of 38.1 ± 7.7 MPa determined by an intrusion test.[25] The particles are glued together by the consolidation.

The porous root replica made of PLGA is fabricated in the analog manner. A sterile polyvinylsiloxane mold was manufactured after tooth extraction by imprinting the root into the polymer (Fig. 1). After crosslinking of the polyvinylsiloxane, the root was extracted, and the mold was filled with sterile

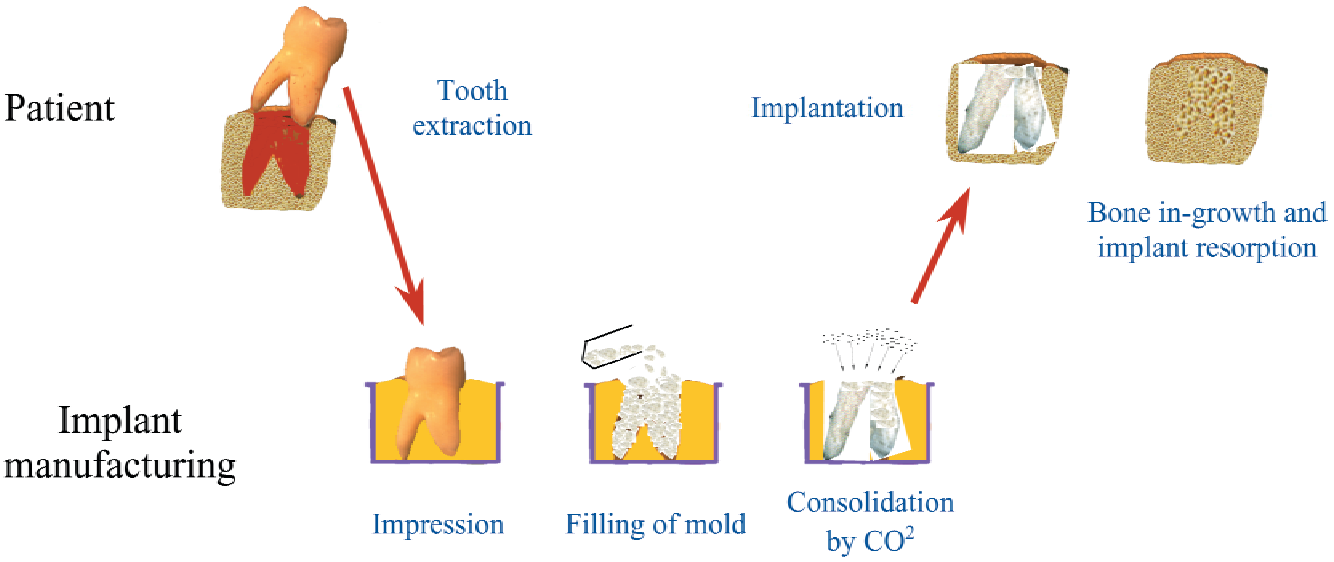

Figure 1. Sequence for the replacement of tooth root by the degradable PLGA implant with interconnected porosity. [Color figure can be viewed in the online issue, which is available at www.interscience.wiley.com.]

PLGA particles having a diameter between 700 and 1400 μm. Using the consolidation method described above, porous root replicas were obtained.

Structural characterization

Scanning electron microscopy (SEM)

The surface topography of the samples was analyzed using SEM (Hitachi S-2500C, Japan). Longitudinal and transversal sections were visualized to reveal the microstructure orientation during consolidation.

Determination of total porosity by gravimetry

The total porosity of the sample Π is defined by the following:

$$\Pi = 1 - \frac{\rho'}{\rho} \tag{1}$$

where ρ is the polymer density [g cm^{-3}] and ρ′ is the integral density of the sample [g cm^{-3}].

The integral density was determined by measuring the weight and the volume of the samples. For these measurements, nine different samples were used. The polymer density was determined by pyknometry on polymers as received. With this integral technique, the total amount of porosity is accessible.

Hg-porosimetry

The intrusion method (Hg-Porosimeter, PMI) was used to determine the open, the closed, and the total porosity as well as the pore sizes distribution. The samples were degassed during 1 h under high-vacuum conditions. The applied Hg-pressure was varied between 0.07 to 2000 bar. The relation between the Hg-pressure P and the radius size of a cylindrical pore r is given by Washburn's equation:

$$P = -\frac{2 \cdot \sigma \cdot \cos\theta}{r} \tag{2}$$

where σ is the surface tension of Hg and θ is the contact angle [deg].

The Hg-surface tension at a temperature of 25°C corresponds to 4.74×10^{-3} Ncm^{-1}.[14] A contact angle θ of 137° for PLGA 85:15 was measured according to the procedure described in Whang et al.[14] The open porosity is given by Equation (3).

$$\pi = \frac{V_i}{V_B} \tag{3}$$

where π is open porosity, V_i is total intrusion volume [cm^3], and V_B is sample volume [cm^3].

The total porosity Π and the closed porosity ω (non-accessible volume for Hg) can be calculated using Equation (1) with:

$$\rho' = \frac{m}{V_B} \tag{4}$$

$$\omega = \Pi - \pi. \tag{5}$$

Image analysis using confocal laser scanning microscopy

As SEM, optical microscopy can only reveal the inner micro-architecture of the scaffold after micro-section preparation. For the analysis of CLSM images, planar sections are required. Therefore, we prepared the samples as follows: first, they were embedded into epoxy resin (Resin and Hardener EPOFIX Struers, DK, ratio 25:3) after degassing for 15 min at a pressure of 200 mbar. The resin was fixed at a temperature of 40°C during 12 h. Scaffold sections were prepared by grinding and polishing using the grinding machine (Struers, DK) and a suitable SiC abrasive paper. Polishing was finally achieved with 1-μm diamond paste.

Planar scaffold sections were visualized with the confocal laser-scanning microscope (LSM 410, Zeiss, D). The obtained images were analyzed using the Image-Pro Plus software (n = 6; Media Cybernetics, Silver Spring, MD). Quadratic images with a size of 512 × 512 pixel having a side length of 4839.2 μm were used for the analysis. Hence, the pixel size was 0.1058 μm. Residual scratches of the grinding process were removed from the images by the (3 × 3) median filter.

Threshold determination

Each pixel of the CLSM images can be attributed to a gray value depending on contrast and brightness. To improve the contrast of the raw data, the "Best Fit" filter option of the software was used. The distribution of the gray values are represented by a histogram, where the x-axis corresponds to the gray scale (0–255) and the y-axis represents the related frequency. Three phases corresponding to the closed porosity, the polymer matrix, and the open porosity were distinguishable. The threshold between the closed porosity and the polymer matrix was determined from 60 images using the related minimum of the histogram. The value for the threshold between the polymer matrix and the open porosity was determined by fitting the histograms using two Gaussians taking their crossing point (see below).

Pore sizes distribution

Because of pore shape, which can be seen as an open surface, no computed measurements could be performed on 2D digital images to determine the pore sizes distribution. For this reason, mean throat length was chosen for the characterization of the distribution and was performed manually with the method of interceptive lines. Ten lines were drawn on CLSM images. The distances between the points, where the lines intercepted the pixels of the scaffold matrix, were measured and the related distribution was calculated.

Image analysis using computed micro-tomography

Measurements were performed on cylindrical scaffolds with a diameter of 5 mm and a height of 3.5 mm. 3D images were generated by synchrotron-radiation-based computed tomography (measurements: monochromatic X-ray energy 9 keV at beamline BW 2; HASYLAB synchrotron facilities at Hamburg, Germany) with a resolution of 5.4 μm.[26] The 3D structure was reconstructed from a series of 2D projections using the BKFIL procedure.[27]

The porosity was determined after calculating the threshold value between the phases (as for CLSM image analysis; see below).[28] In addition, the background noise in the tomogram was reduced by a special filtering process.[28] The open and closed porosities are superimposed because of identical X-ray absorption of air in both phases. The amount of closed porosity was estimated counting the pores and measuring their size using a lab-made computer code, which allows the treatment of a data set of several GB with precision.

RESULTS

Structural characterization on the macro- and the microscopic level

Qualitative results

Using the presented molding technique, it is possible to manufacture open porous scaffolds with the desired shape. As an example, Figure 2 represents a PLGA copy of a tooth root produced according to the procedure described in the scheme of Figure 1.

The first step of the procedure implied the production of PLGA particles. These particles were obtained from PLGA yarns, which can relax under CO_2 pressure (Fig. 3). Using thicker yarns, for example with a diameter of 600 μm instead of 70 μm, no relaxation occurs but the fibers usually foam upon pressure reduction resulting in an unfavorable amount of closed porosity. The molecular alignment, which results from fiber spinning, depends on the ratio between dye and fiber diameter. Consequently, the fiber relaxation is attributed to the randomization of molecular alignment. At high pressure, CO_2 acts as solvent for PLGA and enables the assembly of particles. This process allows scaffold fabrication within a few minutes.

Figure 2. Root replica obtained by consolidation of PLGA fibers under carbon dioxide pressure at room temperature. The length of the root is about 15 mm. [Color figure can be viewed in the online issue, which is available at www.interscience.wiley.com.]

The SEM analysis showed a homogeneous distribution of the pores. Figure 4 demonstrates that the outer shape of the scaffold is identically represented by SEM and 3D CMT, which indicates that the intense X-rays do not damage the scaffold during CMT analysis. The inner structure of the scaffold is investigated without the destruction of the sample using CMT (Fig. 5). The slices of the scaffolds indicate interconnected porosity accessible from outside the sample. The relaxed structure of PLGA fibers is better visible at higher magnification. The inner microstructure observed with CMT is compared with the CLSM results (Fig. 6). However, in the later case, the observation of inner structure requires the destruction of the sample. The preparation procedure used for CLSM investigation seems not to significantly alter the micro-architecture. Closed porosity, corresponding to regions where no light is reflected, can be distinguished, permitting the complete characterization of the porosity of the scaffolds.

Quantitative results

The results of the porosity measurements obtained with gravimetry, Hg-porosimetry, and image analysis are compared in Table I. The total porosity obtained by gravimetry was 69 ± 4%. The standard intrusion method, here Hg-porosimetry, reveals the accessible volume for a specific fluid. The typical pore sizes and shapes of the samples lead to the Hg-penetration of the larger pores having open diameters of about 200 μm without the need of pressure application. For this reason, the large pores cannot be quantified using Hg-porosimetry. The measurement of the PLGA scaffolds with Hg-porosimetry leads to scattered experimental data between 3 and 100 μm that is inherent to the method (Fig. 7). The cumulative representation of intruded volume reveals the presence of pores smaller than 1 μm, which are probably due to compression of the polymer at high Hg-pressure and, therefore, should not be considered in the porosity calculation of connected pores. Hg-porosimetry led to an accessible volume of 60 ± 5%. The total porosity was found to be 65 ± 5%. By including the micro-pores smaller than 1 μm into the calculation, the total porosity resulted in 67%.

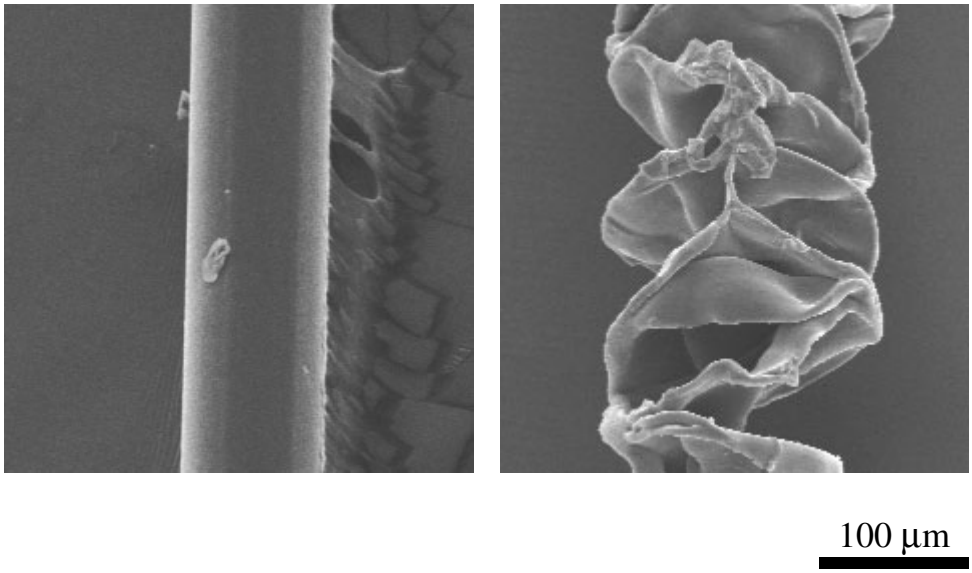

Figure 3. Relaxation of PLGA fibers demonstrated by SEM images. Note the doubling of fiber diameter related to the formation of the porous structure. (a) Plain fiber, (b) porous fiber after relaxation.

On the CLSM images (Fig. 6), one can distinguish between the PLGA scaffold, the epoxy resin, and the holes. The epoxy resin corresponds to the open porosity and the holes to the closed porosity. Each phase covers a range of gray values as shown in Figure 8. The analysis of the closed pores showed that the corresponding gray values range from 0 to 30 (corresponding to a local minimum). Therefore, after analyzing all images, the first threshold value was set to 30. To set the second threshold value to distinguish between polymer and open porosity, the minimum between the second and the third peak was calculated and found at 150.

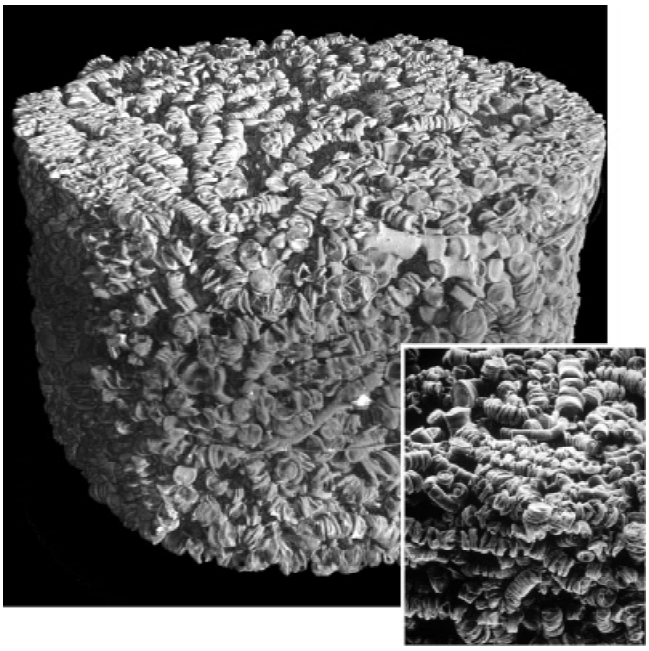

Figure 4. The outer shape of the porous scaffold visualized by CMT and SEM (inset). The comparison between the images reveals that the X-rays from the synchrotron radiation source do not cause visible changes of the porous structure.

The applicability of the computed segmentation method was evaluated using samples made of non-relaxed, non-porous PLGA fibers that are much easier to analyze. Porosity of these samples was first investigated manually by selecting the PLGA phase and by calculating the ratio between the PLGA surface over the overall surface of the image, giving rise to a porosity of 90.47%. Using the computed segmentation method, porosity was found to be 90.02% and after the additional use of a median filter the porosity was 90.41%. The agreement between the results for this rather simple structure should be equally valid for the rather complex structures of the PLGA scaffolds with a total porosity of about 60–65%.

The pore sizes distribution was determined by CLSM images using the method of intercepting lines. The median distance between two points of the PLGA matrix located on the same line was found to be 154 ± 8 μm (Fig. 9).

The CMT measurements allow the determination of the total porosity in 2D and 3D using a similar segmentation method as used for CLSM. Using the 2D slices, a total porosity of 62 ± 2% and a closed porosity of 9.2 ± 0.6% were found. The use of the whole 3D data set leads to a total porosity of 62.7 ± 1.4%, an open porosity of 61.1 ± 5%, and a closed porosity of about 1.5%.

The pore architecture can be quantified by the analysis of the 3D data. For example, one can determine the smallest distance of each voxel to material. The representation allows visualizing, where tissue

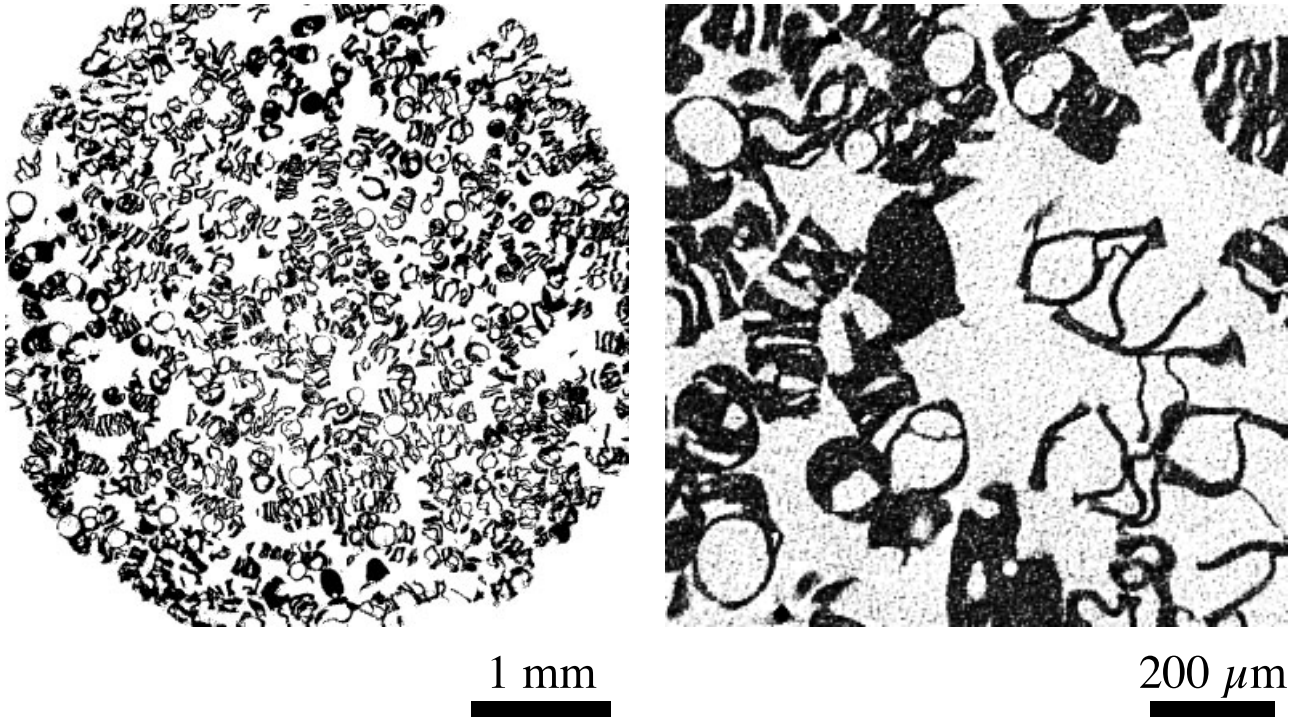

Figure 5. Slices from the tomogram with different magnifications. The complex structure related to the relaxed fibers becomes visible in detail. The slices qualitatively elucidate the high degree of interconnected open porosity. This microarchitecture with a high degree of specific surface should allow cell seeding.

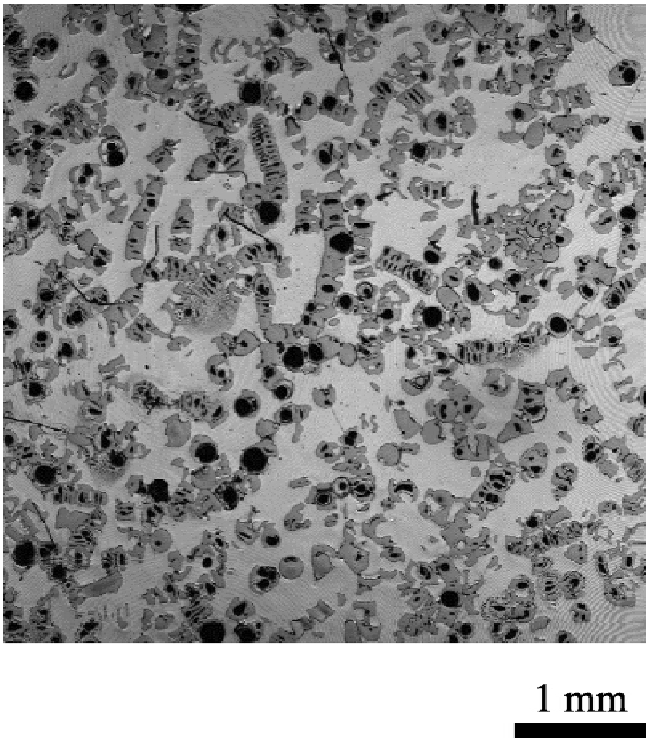

Figure 6. CLSM image of the PLGA scaffold. Note that the structure of the CLSM image closely resembles the CMT data of Figure 5. Epoxy (bright) is considered as the open porosity.

can in-grow by considering blood-capillary-diameters or cell dimensions. Although only a 2D representation is shown in Figure 10, distance mapping considers voxel from above and below. Distance mapping confirmed the presence of interconnected pores. Assuming pores of spherical shape, the mean pore diameters of 100 μm for 3D analysis and 106 μm for 2D analysis are derived from the mean distances to material.[28]

DISCUSSION

The consolidation of PLGA particles using subcritical carbon dioxide permits the manufacturing of defect analogous scaffolds without any time-consuming solvent extraction step. A promising appli-

TABLE I
Summary of the Porosity Measurements of PLGA 85:15 Scaffolds Using Different Methods

Method	Open Porosity (%)	Closed Porosity (%)	Total Porosity (%)
Gravimetry	—	—	69 ± 4
Hg-porosimetry	60 ± 5	5 ± 3	65 ± 5
CLSM 2D	51 ± 3	7 ± 4	58 ± 3
CMT 2D	—	9.2 ± 0.6	62 ± 2
CMT 3D	61.1 ± 5.0	1–2	62.7 ± 1.4

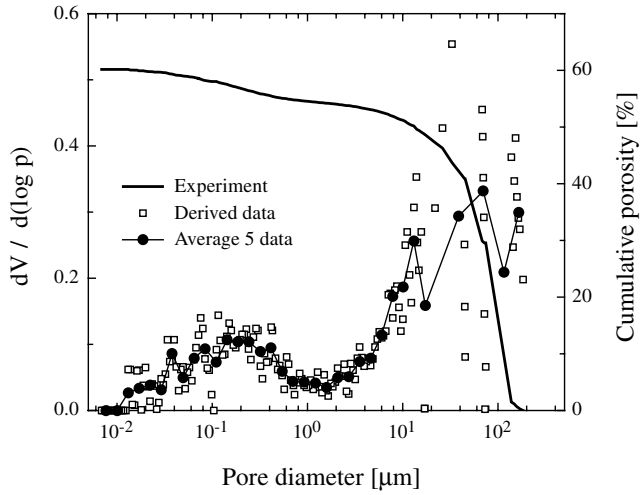

Figure 7. Pore sizes distribution and cumulative open porosity measured by Hg-porosimetry for PLGA scaffolds. The full line (experiment) represents the experimental data, i.e., the cumulative porosity versus pore diameter determined from applied pressure. The pore sizes distribution is found by the derivative dV/d(log p) versus pore diameter (derived data). The pore sizes distribution reveals data scattering for pore diameters larger than 10 μm that is inherent to the method. To guide the eyes, averaged data are also represented. The peak between 0.01 and 1 μm is attributed to the compression of the polymer.

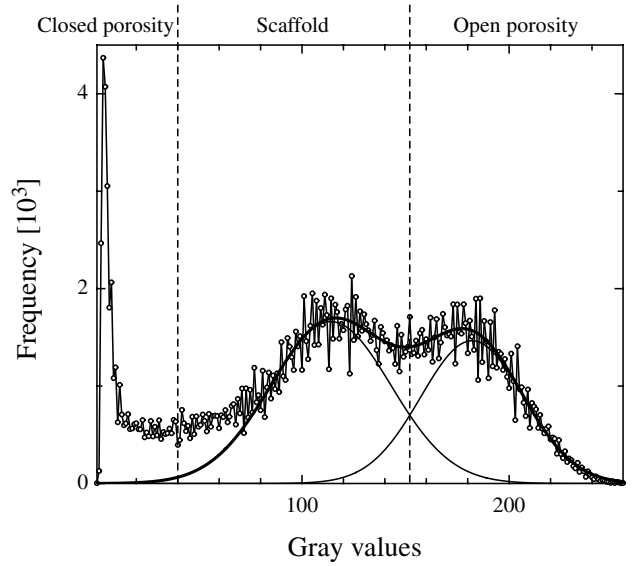

Figure 8. Histogram of the gray values obtained from the CLSM images. The three peaks originate from the PLGA scaffold material, the epoxy (open porosity), and the holes (closed porosity). The threshold between the closed porosity and the scaffold is set to the minimum between the two peaks. The threshold between the scaffold and the open porosity corresponds to the crossing point of two Gaussians fitting the experimental data.

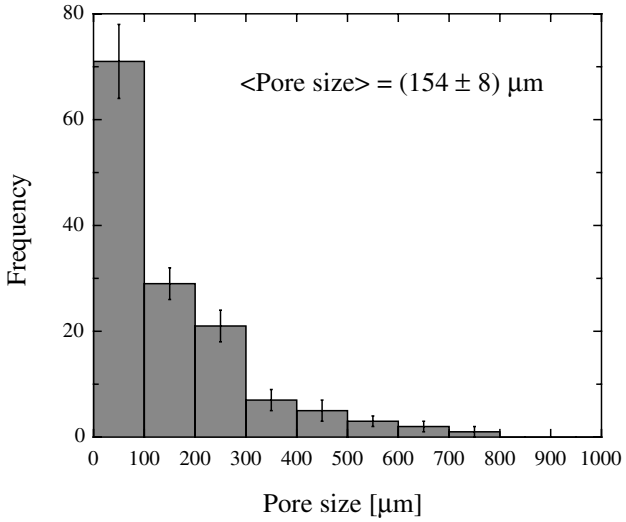

Figure 9. Pore sizes distribution extracted from CLSM images using the distances between two points of the polymer matrix located on the same line and separated by epoxy resin. The median of the distribution was found to be 154 ± 8 μm.

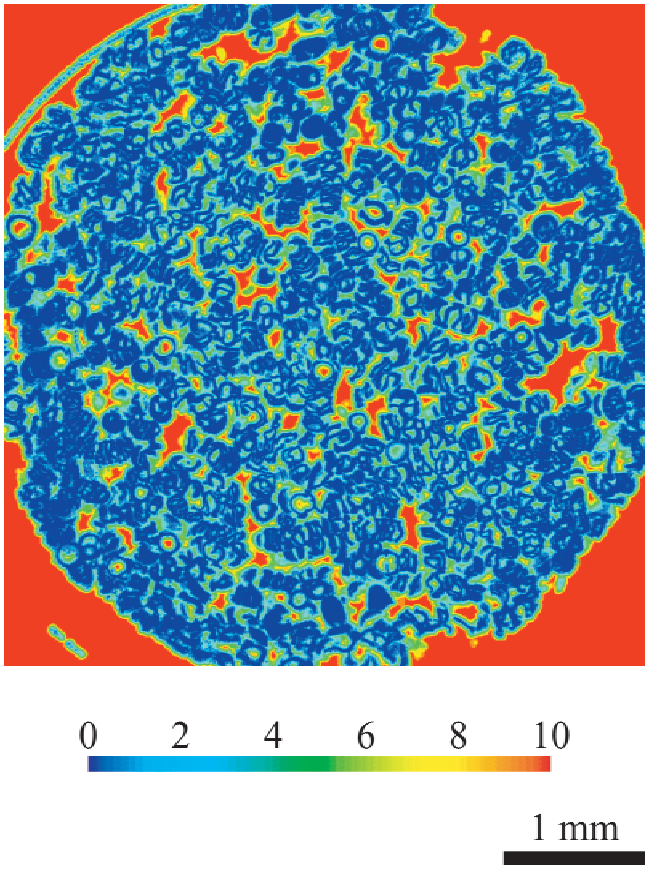

Figure 10. 3D-distance mapping of a tomographic slice. The color table corresponds to the voxel size, i.e., 3.8 μm. The red color represents voxels, which are more than 38 μm apart from PLGA. The blue-colored voxels represent the scaffold itself.

cation of the technique is the fabrication of defect analog scaffolds for tissue augmentation. Here, the implant can be manufactured after tooth extraction with sterile particles directly before implantation. The implant should prevent bacterial contamination of the alveola. Because the implant is a copy of the individual root, the risk of displacement or the loss of the implant is minimized.

To produce porous particles with a high degree of porosity, PLGA fibers are used. After spinning, PLGA molecules are highly orientated. This metastable state of matter is transformed into a more favorable energetic state by relaxing the fibers. Relaxing can be achieved by increasing the temperature above the glass transition temperature T_g of the polymer. Sorbed CO_2 molecules in PLGA are known to reduce the glass transition of the polymer under room temperature.[25] Thus, when PLGA fibers are exposed to CO_2 pressure at room temperature, relaxation of the fibers is observed. In the case of PLGA fibers with diameters smaller or equal to 60–100 μm, relaxation provokes contraction of the fibers and formation of folds, which can be clearly seen on CMT or CLSM images. In preliminary experiments, only formation of bubble-like pores was observed by fibers thicker than about 100 μm without any relaxation effects. Scaffolds made of theses fibers exhibit only a small amount of open porosity.

At high magnification, CMT or CLSM images reveal some bubbles. Their formation seems to depend on diameter irregularities, which provides sites for nucleation and growth of the gas phase.[29] The formation of a gas phase in polymers generally leads to closed pores. Dissolved CO_2 in the polymer matrix temporarily acts as plasticizer and poor solvent.[25] Thus, PLGA particles can assemble, forming a solid structure. After the process, fibers formed a stable interpenetrated network without preferential orientation.

The inner architecture was observed with CLSM, which requires the destruction of the scaffold to prepare slices. Here, we see the advantage of a nondestructive technique such as CMT. Because of their adequate cross-section, synchrotron X-rays are appropriate to nondestructively investigate the microstructure of PLGA scaffolds with a resolution of a few micrometers. As confirmed by the comparison with SEM, the X-rays do not visibly affect the micro-architecture of the scaffolds. Thus, CMT data can be directly compared with CLSM.

Both the image analysis using the CLSM and the CMT data confirmed the presence of interconnected pores throughout the scaffolds. Because of the pore geometry, the entire microstructure of the scaffold is accessible from outside, which would enable its vascularization and the in-growth of different kinds of tissue.

The porosity and the pore sizes distribution of the scaffold were quantified with gravimetry, Hg-porosimetry, and CMT and CLSM images. The gravimetry as an integral method does not distinguish between closed and open porosity. Moreover, the volume measurement of the scaffold is inaccurate. For this reason, the scaffold volume and consequently the total porosity are often overestimated. Hg-porosimetry belongs to the standard methods to quantify the porosity and pore sizes distribution for porous structures. However, as a result of the presence of large pores, Hg penetrates into the scaffold without pressure application. For this reason, the volume of the scaffold is generally underestimated, which leads to a lower value for the open porosity and finally a lower total porosity. Moreover, the pore sizes distribution does not include pores larger than 100 μm (Fig. 7), which are important for potential vascularization. The pore sizes distribution appears to be bimodal, showing a micro- and macro-porosity. A possible explanation for the presence of this micro-porosity is the formation of micro-cavities or a compression of the polymer after mercury penetration into the polymer matrix because of elevated pressure. Consequently, this micro-porosity of about 2% needs to be considered in calculations in an appropriate manner.

Image analysis is expected to lead to more precise results. After noise filtering and thresholding, image segmentation on CLSM slices permits distinction between the polymer matrix, the open, and the closed porosity. The closed porosity can be characterized by the absence of material and, therefore, cannot reflect light. A comparison with CMT tomograms confirms that these bubble-like structures are enclosed within the polymer matrix and do not represent cavities in the epoxy resin. Before porosity quantification, computed segmentation method was assessed using a regular structure. Porosity calculations based on this structure confirm that segmentation was reproducible and, therefore, adequate to characterize the scaffolds. The open, the closed, and the total porosity were analyzed in the central region of the scaffolds. Total porosity determined by CLSM was found to be 58 ± 3%, a value slightly smaller than that found by the other methods used. Because the microstructure consists of a few interconnecting pores, a size distribution is not characteristic. Therefore, a line method is used to characterize the pore diameters. The median values of this distribution can only be used to compare different scaffolds, although it does not characterize the accessibility to the scaffold for the tissue in-growth.

Insufficiencies of CLSM-based image analysis are caused by the difficulty of obtaining uniform brightness on the whole image. The resin (open porous phase) can exhibit the same gray values as the polymer matrix, if the surface is not perfectly aligned to the laser. The segmentation becomes questionable and can lead to an underestimated value of the open porosity.

Another problem can arise from the potentially nonhomogeneous wetting of the scaffolds with the epoxy resin. However, comparison of the CLSM images with the CMT tomograms proves that the interconnected pores of the scaffolds were filled by epoxy. Therefore, the wettability of the liquid resin was adequate for our investigation.

CMT is a superior method to observe the inner structure of the scaffolds nondestructively. Hence, preparation artifacts are avoided and the porosity is derived precisely. Measurements were possible on the 2D slices as well as the whole 3D tomogram. The total porosity obtained with both methods is identical; the value of the closed porosity is statistically higher by 2D image analysis than by 3D analysis. Our explanation for this discrepancy is that some bubble-like pores may have thin orifices, which are registered as open porosity by 3D analysis, but not by 2D analysis. A supplementary advantage of tomography is the possibility of visualizing potential pathways for tissue in-growth. The distance mapping shows that the micro-architecture is mainly composed of narrow interconnected conduits (12.5– 25μm). For optimal bone in-growth into PLGA scaffolds after implantation, it has been stated that pore diameters should be in the range of 300–350 μm in the case of calvarial rat defects.[30] However, no significant difference in osteoblast proliferation and phenotype conservation has been found in PLGA foams with pores sizes of either 150–300, 300–500, or 500–710 μm when seeded with stromal osteoblasts and after implantation into rat mesentery.[10] The average penetration depth of mineralized tissue into the construct seemed to be deeper for scaffolds with pores between 150 and 300 μm than for that with pore sizes between 500 and 710 μm after 49 days *in vivo*.[31] Similar results were found in an *in vitro* study with neonatal rat calvarial osteoblasts.[32] Therefore, PLGA scaffolds presented in this report should be optimized to deliver a large amount of wider pores for bone defect regeneration.

We gratefully acknowledge the CMT measurements of Felix Beckmann (Hamburger Synchrotronstrahlungslabor HASYLAB at Deutsches Elektronen-Synchrotron DESY) and the support of 3D data evaluation of Marius Huser and Gábor Székely (ETH Zürich).

References

1. Atwood D. Reduction of residual ridges: A major oral disease entity. J Prosthet Dent 1971;26:266–279.
2. Yoshikawa M, Toda T. Reconstruction of alveolar bone defect by calcium phosphate compounds. J Biomed Mater Res 2000; 53:430–437.
3. Mecall RA, Rosenfeld AL. Influence of residual ridge resorption patterns on fixture placement and tooth position. Part III. Presurgical assessment of ridge augmentation requirements. Int J Periodontics Restorative Dent 1996;16:322–337.
4. de Groot K. Dental implants. In: de Groot K, editor. Bioceramics of calcium phosphate. Boca Raton, FL: CRC Press; 1983. p 116–129.
5. Denissen HW, de Groot K. Immediate dental root implants from synthetic dense calcium hydroxylapatite. J Prosthet Dent 1979;42:551–556.
6. Bell DH. Particles versus solid forms of hydroxyapatite as a treatment modality to preserve residual alveolar ridges. J Prosthet Dent 1986;56:322–326.
7. Suhonen JT, Meyer BJ. Polylactic acid (PLA) root replica in ridge maintenance after loss of a vertically fractured incisor. Endod Dent Traumatol 1996;12:155–160.
8. Ishaug SL, Yaszemski MJ, Bizios R, Mikos AG. Osteoblast function on synthetic biodegradable polymer. J Biomed Mater Res 1994;28:1445–1453.
9. Bostrom RD, Mikos AG. Tissue engineering of bone. In: Atala A, Mooney DJ, editors. Synthetic biodegradable polymer scaffolds. Boston: Birkhäuser; 1997. p 215–234.
10. Ishaug SL, Crane GM, Miller MJ, Yasko AW, Yaszemski MJ, Mikos AG. Bone formation by three-dimensional stromal osteoblast culture in biodegradable polymer scaffolds. J Biomed Mater Res 1997;36:17–28.
11. Park SH, Llinas A, Goel VK, Keller JC. Hard tissue replacements. In: Bronzino JD, editor. The biomedical engineering handbook. Boca Raton, FL: CRC Press; 1995. p 672–703.
12. Ruffieux K. Degradables osteosynthesesystem aus polylactid für die maxillofaciale chirurgie. Ph.D. Thesis ETH Zürich, Zürich; 1997.
13. Rozema FR. Resorbable poly(L-lactide) bone plates and screws: Tests and applications. Ph.D. Thesis, Groeningen; 1991.
14. Whang K, Thomas CH, Healy KE. A novel method to fabricate bioabsorbable scaffolds. Polymer 1995;36:837–842.
15. Lin SS, Ueng SW, Liu SJ, Chan EC, Chao EK, Tsai CH. Development of biodegradable antibiotic delivery system. Clin Orthop 1999;362:240–250.
16. Goldstein AS, Zhu G, Morris GE, Meszlenyi RK, Mikos AG. Effect of osteoblastic culture conditions on structure of poly(D,L-lactic-*co*-glycolic acid) foam scaffolds. Tissue Eng 1999;5:421–433.
17. Rotter N, Aigner J, Naumann A, Planck H, Hammer C, Burmeister G. Cartilage reconstruction in head and neck surgery: Comparison of resorbable polymer scaffolds for tissue engineering of human septal cartilage. J Biomed Mater Res 1998; 42:347–356.
18. Sittinger M, Perka C, Schultz O, Häupl T, Burmeister GR. From cartilage metabolism to clinics: Joint cartilage regeneration by tissue engineering. Z Rheumatol 1999;58:130–135.
19. Mikos AG, Thorsen AJ, Czerwonka LA, Bao Y, Langer R, Winslow DN. Preparation and characterization of poly(L-lactic acid) foams. Polymer 1994;35:1068–1077.
20. Nam YS, Park TG. Biodegradable polymeric microcellular foams by modified thermally induced phase separation method. Biomaterials 1999;20:1783–1790.
21. Agrawal CM, Kennedy ME, Micallef DM. The effects of ultrasound irradiation on a biodegradable 50–50% copolymer of polylactic and polyglycolic acids. J Biomed Mater Res 1994;28: 851–859.
22. Athanasiou KA, Schmitz JP, Agrawal CM. The effect of porosity on *in vitro* degradation of polylactic acid–polyglycolic acid implants used in repair of articular cartilage. Tissue Eng 1998; 4:53–63.
23. Harris LD, Kim BS, Mooney DJ. Open pore biodegradable matrices formed with gas foaming. J Biomed Mater Res 1998;42: 396–402.
24. Schug J. Medical implant. European Patent No. EP893975A1; 1996.

25. Maspero FA. Biodegradable, open porous scaffolds for the prevention of alveolar bone loss after tooth extraction: CO_2-processing and *in vitro* behavior. Ph.D. Thesis 14270, ETH Zürich, Zürich; 2001.
26. (a) Beckmann F, Müller B, Maspero F, Ruffieux K, Wintermantel E. Computed micro-tomography of porous polymers. HASYLAB annual report. Part 1. Imaging techniques. 1999. p 887–888. (b) Müller B, Thurner P, Beckman F, Weitkamp T, Rau C, Bernhardt R, Karamuk E, Eckert L, Buchloh S, Wintermantel E, Scharnweber D, Worch H. Three-dimensional evaluation of biocompatible materials by microtomography using synchrotron radiation. Proc SPIE 2002;4503:178–188.
27. Herman GT. Image reconstruction from projections: Implementation and applications. Berlin: Springer; 1979.
28. Müller B, Beckmann F, Huser M, Maspero F, Szekely G, Ruffieux K, Thurner P, Wintermantel E. Non-destructive three-dimensional evaluation of a polymer sponge by microtomography using synchrotron radiation. Biomol Eng. To appear.
29. Mooney DJ, Baldwin DF, Suh NP, Vacanti JP, Langer R. Novel approach to fabricate porous sponges of poly(D,L-lactic-*co*-glycolic acid) without the use of organic solvents. Biomaterials 1996;17:1417–1422.
30. Robinson B, Hollinger HO, Szachowicz E, Brekke J. Calvarial bone repair with porous D,L-polylactide. Otolaryngol Head Neck Surg 1995;112:707–713.
31. Ishaug-Riley SL, Crane GM, Gurlek A, Miller MJ, Yasko AW, Yaszemski MJ. Ectopic bone formation by marrow stromal osteoblast transplantation using poly(D,L-lactic-*co*-glycolic acid) foams implanted into the rat mesentery. J Biomed Mater Res 1997;36:1–8.
32. Ishaug-Riley SL, Crane-Kruger GM, Yaszemski MJ, Mikos AG. Three-dimensional culture of rat calvarial osteoblasts in porous biodegradable polymers. Biomaterials 1998;19:1405–1412.